Stopping and straggling of 60–250-keV backscattered protons on nanometric Pt films

F. F. Selau,[1,*] H. Trombini,[1] G. G. Marmitt,[2] A. M. H. de Andrade,[1] J. Morais,[1] P. L. Grande,[1] I. Alencar,[3] M. Vos,[4] and R. Heller[5]

[1]*Instituto de Física, Universidade Federal do Rio Grande do Sul (UFRGS), Av. Bento Gonalves 9500, CEP 91501-970, Porto Alegre, RS, Brazil*

[2]*Department of Radiation Oncology, University Medical Center of Groningen, University of Groningen, 9713 GZ Groningen, The Netherlands*

[3]*Departamento de Fsica, Universidade Federal de Santa Catarina (UFSC), CEP 88040-900, Florianópolis, SC, Brazil*

[4]*Electronics Materials Engineering, Research School of Physics, The Australian National University (ANU), ACT 0200, Canberra, Australia*

[5]*Institute of Ion Beam Physics and Materials Research, Helmholtz-Zentrum Dresden-Rossendorf e.V. (HZDR), D-01328, Dresden, Germany*

(Received 9 June 2020; revised 29 July 2020; accepted 7 August 2020; published 14 September 2020)

The stopping power and straggling of backscattered protons on nanometric Pt films were measured at low to medium energies (60–250 keV) by using the medium-energy ion scattering technique. The stopping power results are in good agreement with the most recent measurements by Primetzhofer Phys. Rev. B **86**, 094102 (2012) and are well described by the free electron gas model at low projectile energies. Nevertheless, the straggling results are strongly underestimated by well-established formulas up to a factor of two. Alternatively, we propose a model for the energy-loss straggling that takes into account the inhomogeneous electron-gas response, based on the electron-loss function of the material, along with bunching effects. This approach yields remarkable agreement with the experimental data, indicating that the observed enhancement in energy-loss straggling is due to bunching effects in an inhomogeneous electron system. Nonlinear effects are of minor importance for the energy-loss straggling.

DOI: 10.1103/PhysRevA.102.032812

I. INTRODUCTION

The electronic stopping power is a fundamental quantity describing the interaction of ionizing ions with matter. It is a key parameter in a broad spectrum of applications, ranging from ion-beam analysis [1] to hadron therapy [2]. For all current applications the precise knowledge of the energy-loss per distance traveled by the ion (so-called stopping power) and its corresponding variance (so-called energy-loss straggling) are of crucial importance. Notably, in the case of ion velocities of the order of the Bohr velocity (about $c/137$) the existing models are not accurate enough to meet the needs of many different applications. This is particularly true for the energy-loss straggling used in medium-energy ion scattering (MEIS) experiments, where this parameter is important for the interpretation of spectra of thin films [3,4] and for the size determination of nanostructures composed of heavy metals [5,6]. In addition, metals such as platinum (Pt) have few and contradictory experimental stopping results for medium-energy ions [7]. This metal is one of the most relevant transition metals in heterogeneous catalysis, where it is mostly used in the form of nanometric clusters. For instance, it is a catalyst for the conversion of NO, a main component of the air pollution [8], into N_2 and O_2 [9]. MEIS is a powerful tool to determine the inner structure of nanoparticles [6], and more precise data on energy-loss straggling are required to expand the use of MEIS to better characterize Pt-based catalysts.

In this work we investigate the stopping power and energy-loss straggling of medium-energy H^+ ions in a planar system of Pt nanofilms deposited on silicon dioxide (SiO_2) over a silicon (Si) substrate. The Pt layer was independently characterized by transmission electron microscopy (TEM), x-ray reflectivity (XRR), Coulomb explosion depth profiling [10–13], and atomic force microscopy (AFM). In addition, the areal density of the Pt atoms was evaluated by Rutherford backscattering spectrometry (RBS). The parameters obtained from these measurements were fixed in the simulations of the MEIS spectra to extract the stopping power and energy-loss straggling of the Pt layer as a function of the projectile energy. These data are compared with predictions of different models of stopping and straggling. Particularly, for the energy-loss straggling, a model is developed here that takes into account the electron response based on the electron-loss function (ELF) of the material, similar to a recent approach proposed for stopping-power calculations [14]. In addition, the bunching effect [15] due to spatial correlation in electron-density inhomogeneities was taken into account.

This work is organized as follows: In Sec. II we present the procedure of synthesis and characterization of samples and the main experimental techniques used in this work. Then, in Sec. III, the theoretical model of energy-loss straggling is described in detail. Finally, we present and discuss the results obtained for the stopping power and energy-loss straggling analysis for low- to medium-energy protons on Pt in Sec. IV. Atomic units [$m_e = 1$, $\hbar = 1$ and $e^2/(4\pi\epsilon_0) = 1$] and nonrelativistic expressions are used throughout this work, unless stated otherwise.

*felipe.selau@ufrgs.br

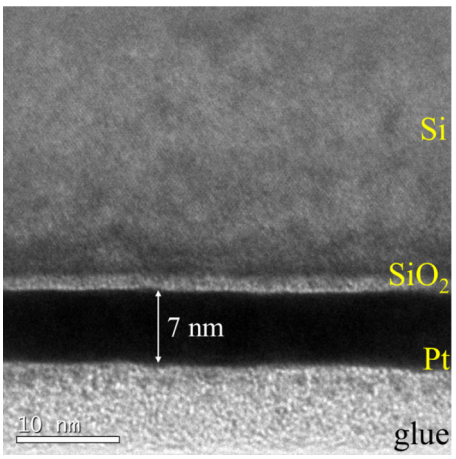

FIG. 1. TEM cross-section image of the $Pt/SiO_2/Si$ (sample A) measured at the CMM of UFRGS.

II. EXPERIMENTAL PROCEDURE

Two sets of samples (A and B) were prepared by the DC sputtering technique at the Nanometric Conformation Laboratory (NCL) of the Federal University of Rio Grande do Sul (UFRGS) for MEIS analysis using two different facilities: at the ion beam laboratory of the UFRGS (sample A) and at the Helmholtz-Zentrum Dresden-Rossendorf (HZDR; sample B). The Pt was deposited on a native SiO_2/Si (100) substrate (sample A) and on a thermally grown SiO_2 (90 nm)/Si (100) substrate (sample B). The Pt thicknesses for sample A and B were 7 and 20 nm, respectively. Using these two samples we were able to investigate the influence of sample thickness on the stopping power and energy-loss straggling measurements. The actual thickness and roughness of samples were measured with different techniques (TEM, AFM, XRR). In addition, the total number of Pt atoms per cm^2 was measured by the RBS technique. The characterization procedure for each sample is explained in what follows.

Sample A was analyzed by TEM (Fig. 1) using a JEOL 2010 microscope operating at 200 kV from the Center for Microscopy and Microanalysis (CMM) at UFRGS. The sample was cut, glued, and thinned by using mechanical polishing and ion milling. The thickness of the Pt layer was found to be 7.0 ± 0.3 nm. The corresponding uncertainty was determined from the instrumental precision of 3% and the standard deviation measured for different magnifications of the same region. This value was in agreement with measurements by the Coulomb explosion technique, using a molecular beam to provide the actual thickness of sample (see Supplemental Material [16] for the description of this technique). The thickness (obtained by TEM) of the Pt layer and the areal atomic density N (obtained by RBS) [17] were used to obtain the layer density. The result is about 12% smaller than the Pt bulk density. This method has been used to evaluate thin-film densities in the literature [18,19]. This density value of 18.9 g/cm^3 was then used to simulate the MEIS measurements performed at the UFRGS. The decrease in film density is well established in the literature due to, e.g., a porous microstructure and voids [19].

Sample B was analyzed by XRR at the NCL. The corresponding thickness of the Pt layer was 19.5 ± 0.4 nm.

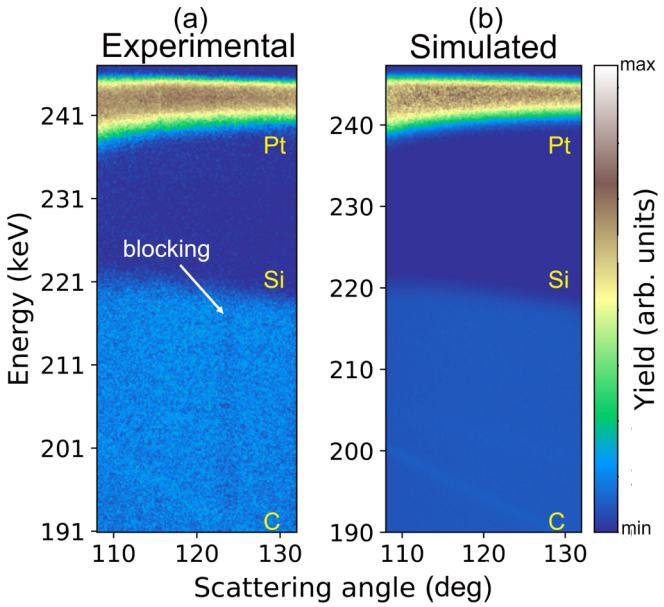

FIG. 2. (a) Experimental and (b) simulated 2D-MEIS spectra taken with 250 keV H^+ and normal incidence for sample A. The colors represent the backscattering yield on a log scale.

Such a thickness together with RBS measurements for the total number of Pt atoms per cm^2 provided a layer density that is close to the Pt bulk density (21.45 g/cm^3). This density value was then used to simulate the MEIS measurements performed at the HZDR. Further details of the thickness and density determination are in the Supplemental Material [16].

The ion-scattering measurements were performed at two MEIS facilities (UFRGS and HZDR). In both labs an electrostatic accelerator provided a normal incident beam of H^+ with energies ranging from 60 to 250 keV at UFRGS and 60 to 120 keV at HZDR. In the two labs the backscattered H^+ ions were analyzed with a toroidal electrostatic analyzer (TEA). At the exit plane of the TEA, a pair of microchannel plates coupled to a position-sensitive detector was used to measure the energy and angle for the scattered ions [20,21]. The samples were loaded in each MEIS chamber without any further treatment. The UFRGS (HZDR) analyzer, with angular aperture of 24 degrees (29 degrees), was mounted at 120 degrees (118 degrees) with respect to the incident beam. A two-dimensional (2D) map of ion scattering yield as a function of the energy and angles was measured in both systems. The overall energy resolution of each system was 4.5×10^{-3} and 2.1×10^{-3} for UFRGS and HZDR, respectively.

Figure 2 presents the 2D MEIS map of ion yield as a function of ion energy and angle taken with 250 keV H^+ for ions impinging on sample A at normal incidence. Because of the large difference between the Pt and Si masses both signals are well separated for this ion energy as indicated in Fig. 2. All MEIS spectra were analyzed with the PowerMEIS-3 (PM3) software [22–24]. This software uses a Monte Carlo algorithm that performs simulations of the interaction of ions (and electrons) with matter. The program includes multiple scattering (MS) and is based on reliable scattering cross sections. Since neutralized ions cannot be measured by the TEA, we included

the neutralization correction from the Marion equation [25] in the simulations.

For all PM3 simulations we used the Pt thickness of 7.0 nm (19.45 nm) and density of 18.9 g/cm^3 (20.8 g/cm^3) for sample A (B) and varied the stopping power and energy-loss straggling to get the best fit of the measurements for three scattering angles. In addition, a small amount of carbon (less than 2 nm) was included on top of the sample to simulate the effect of hydrocarbon contamination (visible for backscattering energies below 200 keV marked by "C"). It caused a small overall shift in the energy spectrum and a maximum broadening of about 180 eV, which had a very small influence on the present results. Such methodology allowed for the determination of the stopping power and energy-loss straggling values for each projectile energy.

III. THEORETICAL PROCEDURE

The free electron gas (FEG) model is a simple but powerful approach to describe the energy loss of ions in solids [15,26,27]. At very low projectile energies only the valence-band electrons contribute to the stopping and straggling values. For quasi-free-electron metals these electrons can be modeled by a homogeneous electron system using the electron density or plasmon energy. For increasing projectile energies other electrons with different densities and larger binding energies come into play, giving rise to the remarkable effects discussed recently by Sortica *et al.* [28] and Matias *et al.* [29]. In general, the valence-band electrons have to be treated as an inhomogeneous electron-gas system composed as a superposition of electron gases with different local densities [29]. For all target electrons Bonderup and Hvelplund [30] used the local-density approximation to evaluate the straggling based on the Lindhard formula [31], which relies on the linear approximation for the interaction of the projectile with the electrons from the medium. Vos and Grande proposed recently [14] a nonlinear scheme based on an extension of the dielectric function model to describe the energy-loss of ions in solids. In this method, the energy loss is calculated for a statistical ensemble of FEGs with different plasmon energies, as suggested by Penn [32] in the context of the electron inelastic mean-free path. For each density the momentum transfer rate from the electrons to the ion [the transport cross section (TCS)] is calculated by using a self-consistent screened electron-ion potential, which provides a nonlinear method to calculate stopping and straggling values.

Specifically, in this model, called here the TCS-Penn model, each electron-gas density is weighted according to the loss function of the material in the optical limit as

$$g(\omega_p) = \frac{2}{\pi\omega_p}\mathrm{ELF}(\omega_p), \tag{1}$$

where $\mathrm{ELF}(\omega)$ is given in terms of the dielectric function of the material as $\mathrm{Im}[-1/\epsilon(\omega, q=0)]$. Each electron-gas contribution is described by the plasmon energy ω_p obtained from the electron-gas density n or equivalently from the radius of a sphere whose volume is equal to the volume per free electron (Wigner-Seitz radius r_s) as $\omega_p = \sqrt{4\pi n} = \sqrt{3}r_s^{-3/2}$. The stopping power for a projectile charge Z_1 is then given by [14]

$$S_{\text{TCS-Penn}} = \int_0^\infty d\omega_p g(\omega_p) S_{\text{TCS}}(Z_1, \omega_p), \tag{2}$$

with the stopping power $S_{\text{TCS}}(Z_1, \omega_p)$ given in terms of the transport cross section σ_{tr} according to [26]

$$S_{\text{TCS}}(Z_1, \omega_p) = \left\langle \frac{|\vec{v}_e - \vec{v}|}{v}\vec{v}\cdot(\vec{v}-\vec{v}_e)\sigma_{tr}(|\vec{v}_e-\vec{v}|)\right\rangle_{\vec{v}_e}, \tag{3}$$

where $\vec{v}$ is the ion velocity and $\langle\ldots\rangle$ stands for the average over the electron velocities $\vec{v}_e$ according to the distribution of a degenerate electron gas with Fermi velocity determined from r_s [26].

In the original Penn approach, the dielectric function and thus the stopping is calculated for each density fraction and is evaluated based on linear (first Born-type) theory. Here we still use a density fraction based on the dielectric function but go beyond first order by evaluating the stopping of a FEG based on the transport cross section σ_{tr}. It is evaluated in the frame where the projectile is at rest and the target electrons are moving. As usual, a central potential is assumed for the electron scattering off the ion, allowing for the well-established partial-wave analysis [26]. Thus, $\sigma_{tr}(k)$ can be expressed by phase shifts δ_ℓ at the relative speed v', according to [26]

$$\begin{aligned}\sigma_{tr}(v') &= \int [1-\cos(\theta)]d\sigma(\theta)\\ &= \frac{4\pi}{v'^2}\sum_{\ell=0}^{\infty}(\ell+1)\sin^2(\delta_\ell-\delta_{\ell+1}).\end{aligned} \tag{4}$$

We used the Yukawa potential for the electron-ion potential with a velocity-dependent screening-length (α^{-1}) from Ref. [33], which is an interpolation between the high ion velocity $\alpha = \omega_p/v$ and α_0 for $v \to 0$ determined from the static Friedel sum rule [34].

Here we extend the above concept to the energy-loss straggling Ω^2 [energy^2/distance] by using

$$\Omega^2_{\text{TCS-Penn}} = \int_0^\infty d\omega_p g(\omega_p)\Omega^2_{\text{TCS}}(Z_1, \omega_p), \tag{5}$$

with the straggling $\Omega^2_{\text{TCS}}(Z_1, \omega_p)$ given in terms of the transport cross sections σ_{tr} and σ_{tr2} according to [15]

$$\begin{aligned}\Omega^2_{\text{TCS}}(Z_1, \omega_p) = \Big\langle n\frac{|\vec{v}_e-\vec{v}|}{v}\Big\{&(v^2-\vec{v}\cdot\vec{v}_e)^2\\ &-\frac{1}{2}\big[v^2v_e^2-(\vec{v}\cdot\vec{v}_e)^2\big]\sigma_{tr2}(|\vec{v}_e-\vec{v}|)\\ &+\big[v^2v_e^2-(\vec{v}\cdot\vec{v}_e)^2\big]\sigma_{tr}(|\vec{v}_e-\vec{v}|)\Big\}\Big\rangle_{\vec{v}_e},\end{aligned} \tag{6}$$

where n is the electron-gas density ($4\pi n = \omega_p^2$) and σ_{tr2} is given by [15,26,35]

$$\begin{aligned}\sigma_{tr2}(v') &= \int [1-\cos(\theta)]^2 d\sigma(\theta)\\ &= \frac{4\pi}{v'^2}\sum_{\ell=0}^{\infty}(\ell+1)\Big[2\sin^2(\delta_\ell-\delta_{\ell+1})\\ &\quad -\frac{\ell+2}{2\ell+3}\sin^2(\delta_\ell-\delta_{\ell+2})\Big].\end{aligned} \tag{7}$$

For a degenerate electron gas, a full and more detailed expression of the straggling cross section $W_{\mathrm{TCS}} = \Omega^2_{\mathrm{TCS}}/n$ is given in Ref. [36] as well as the corresponding correction for the Pauli principle. This correction basically affects the energy-loss straggling at low energies, giving rise to an energy-loss straggling vanishing as v^2 instead of v for $v \to 0$. The results from Eq. (6) are corrected in what follows for the Pauli Principle, as described in Ref. [36].

To get numerical values of the stopping and straggling for Pt we need a description of the ELF. Werner *et al.* published an estimate for the valence-band region based on a reflection electron energy loss experiment [37]. The use of this dielectric function results in an underestimation of stopping and straggling as the contribution of core electrons is significant. Sun *et al.* published a parametrization of the ELF up to 2 keV [38] based on optical data from Weaver [39], Hunter *et al.* [40], and Henke [41]. This parametrization was used in the following results.

For an inhomogeneous electron system there is an additional source of energy-loss straggling called the bunching effect [15,42] and caused by the spatial distribution of the electrons in each atom. Indeed, the energy-loss straggling for an inhomogeneous electron system such as an atom with different shells is not the same as for a homogeneous system with the same average density. Calculations of this effect for light ions were first reported by Besenbacher *et al.* [42]. This contribution is typically important for projectile energies close to the maximum of the stopping power and has been investigated only in a few systems [15,43–45]. It depends on the impact-parameter-dependent mean energy loss $T(b)$ in ion-atom collisions and, as shown in Ref. [45], the additional straggling cross section (ΔW_b) reads according to the independent-electron model:

$$(\Delta W_b) = \int d^2b \left(\sum_i f_i \, T_i(b) \right)^2 - \sum_i f_i \int d^2b \; T_i(b)^2, \quad (8)$$

where f_i is the number of electrons in the ith shell and T_i is the mean energy loss of an electron in the ith shell. The energy-loss straggling due to the bunching effect ($\Delta\Omega^2_b$) was then calculated from Eq. (8) times the Pt density. In what follows we calculated the bunching effect from Eq. (8) by using the shell-wise mean energy loss $T_i(b)$ per electron obtained from the CASP program [46]. It is pointed out that the CASP program cannot be used to calculate the usual uncorrelated straggling contribution.

IV. RESULTS AND DISCUSSION

By using the thickness and density as determined independently by other techniques, each MEIS energy-spectrum was fit to the corresponding experimental result by varying the stopping and straggling parameters. For this sake we used three different scattering angles, which were simulated by using the same stopping power and energy-loss straggling values. In Fig. 3 we present the experimental data and corresponding simulations for sample A at 60 and 250 keV. See the Supplemental Material [16] for other energies and angles measured at HZDR and UFRGS. In addition, the measurements were simulated with and without multiple-scattering

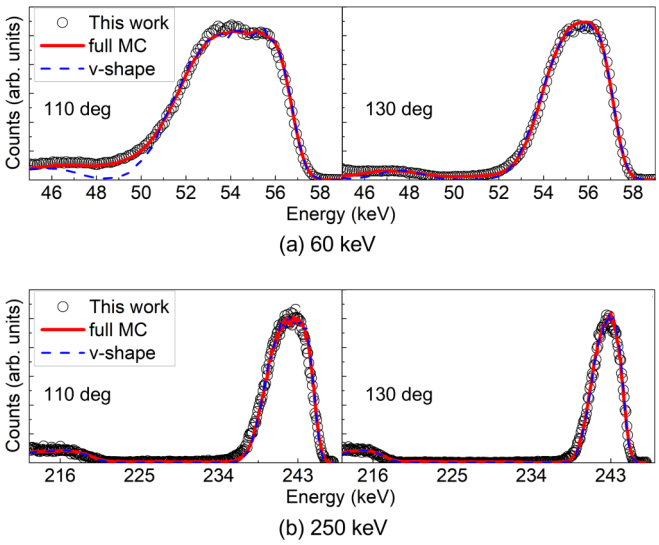

FIG. 3. MEIS spectra as measured at UFRGS for two scattering angles (110 and 130 degrees) and two projectile energies: (a) 60 keV and (b) 250 keV. The black circles represent the experimental data for sample A. The lines are the best-fit simulations obtained from PM3 without (blue line) and with (red line) multiple scattering.

events. The latter implies straight-line trajectories of the ions before and after the backscattering collisions (the v-shape model) whereas the former is full Monte Carlo calculations, based on a variation on the trajectory-reversal approach to connect incoming and outgoing ion trajectories [23]. One set of ion trajectories is simulated for ions impinging on the sample and another set of ions emerging from the analyzer to be connected. An inspection in Fig. 3 shows a much stronger contribution of multiple-scattering collisions at 60 keV compared with 250 keV. Particularly at 60 keV, the Pt and Si signals overlap at 110 degrees and therefore the corresponding energy rear and front edges are not distinguishable anymore.

The stopping power results from full Monte Carlo (MC) simulations are depicted in Fig. 4 with other experimental results and theoretical models (see figure caption for details). The stopping results obtained for samples A and B agree with each other, showing good reproducibility of the method for different samples and MEIS facilities. Both results for sample A and B are in good agreement with the most recent ones from Refs. [50,60] measured by time-of-flight MEIS and ICRU49 [53] values. However, they are about 20% larger than other previous experiments and SRIM [54,55] values. The TCS-Penn results agree with present experimental data and Ref. [50] data at low energies (below 80 keV) within 5% but disagree with the present experimental data for higher energies, reaching 15% at 250 keV. The origin of this discrepancy is not clear and may be related to the accuracy of the Pt loss function employed here. As expected, the TCS-Penn results converge to FEG values (DFT) from Ref. [50] at very low projectile energies since this last approach used an electron density obtained from the plasmon peak as described by the ELF from Sun *et al.* [38]. In fact, the agreement of the TCS-Penn model with the most recent experimental data is rather good at low energies, where the loss function of Pt is dominated by the plasmon contribution. For higher energies,

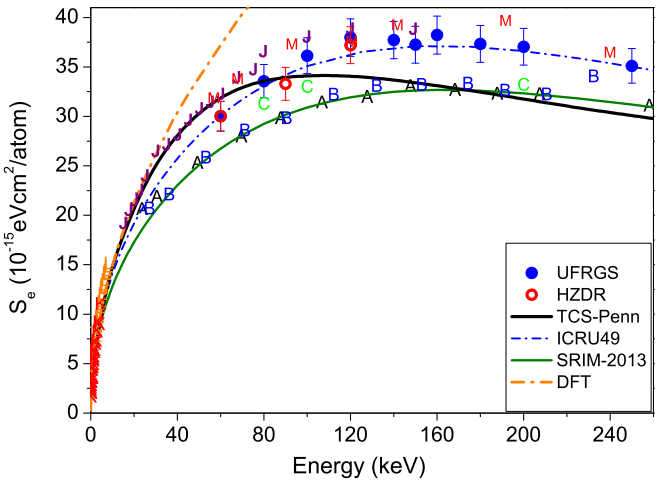

FIG. 4. Stopping cross section for H^+ on Pt. Previous experimental data are described by letters taken from Ref. [7] (A: Ref. [47]; B: Ref. [48]; C: Ref. [49]; J: Ref. [50]; K: Ref. [51]; L: Ref. [52]; M: Ref. [60]). The symbols correspond to the present stopping results obtained from full Monte Carlo (MC) simulations. Blue and yellow dash-dotted curves correspond to ICRU49 [53] and TCS calculations using the DFT potential as extracted from Ref. [50]. Solid black and green lines correspond to the present TCS-Penn model and SRIM [54,55] calculations, respectively.

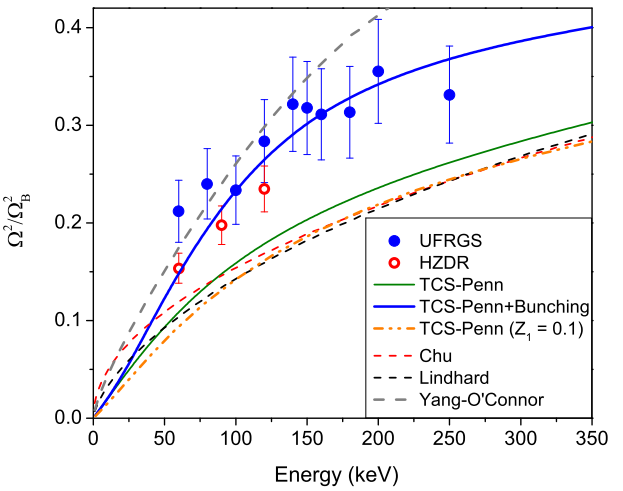

FIG. 5. Energy-loss straggling of H^+ on Pt as a function of energy (60 to 250 keV) divided by the Bohr value $\Omega_B^2 = 2.03 \times 10^{-11}$ eV^2 cm^2. The symbols correspond to the present energy-loss straggling results obtained from full MC simulations for sample A (blue dots) and sample B (red circles). Green and blue solid lines correspond to TCS-Penn and TCS-Penn with bunching effect models, respectively. The dash-dot-dot curve corresponds to TCS-Penn with $Z_1 = 0.1$. The dashes curves correspond to energy-loss straggling obtained for Chu (red), Lindhard (black), and Yang-O'Connor (gray) models. The uncorrelated straggling (TCS-Penn calculation) amounts to 67% of the experimental one at 100 keV/u.

other structures of the loss function come into play, which come from interband transitions involving shallow and inner shells. The use of a FEG-based theory for these transitions is more approximate and an error of the order of 10% is not unexpected.

Figure 5 shows the energy-loss straggling results as extracted from the MEIS spectra for samples A and B as a function of the projectile energy. The error bars stem from variations that corresponded to the best fit of the spectra at different scattering angles. The results of the energy-loss straggling obtained from full Monte Carlo simulations are systematically smaller than those from v-shape simulations. This is because multiple scattering collisions increase the path length of ions along the incoming and exit trajectories, leading to a broadening of the energy-loss spectrum.

The effect of nonuniformities in sample thickness was taken into account according to [15]

$$\Omega^2_{\text{exp.corr.}} = \Omega^2_{\text{sim}} - S^2\delta^2/t, \tag{9}$$

where Ω^2_{sim} is the straggling value obtained from the MEIS simulations, S is the stopping power, δ^2 is the variance for total traveled thickness t (sample roughness). Here the total traveled thickness is about three times the sample thickness due to the geometry. The typical roughness and sample thickness variation is about 0.35 nm as determined by TEM, AFM (sample A), and XRR (sample B) measurements. The corrected values $\Omega^2_{\text{exp.corr.}}$ using the stopping-power values determined from the measurements for each energy are shown in Fig. 5. As for the stopping results, the straggling values for samples A and B agree mostly with each other although the samples thicknesses were quite different. It is pointed out that Kido and Koshikawa [56] have measured the energy-loss straggling for H^+ ions in Cu, Ag, and Pt, but their results are too small and at variance with all other experimental data and, consequently, the results are not included in the figure presented here. An analysis of their published MEIS spectrum with different MEIS simulation programs gives results close to the present ones.

As can be observed in Fig. 5, the present experimental results are much larger than predicted by frequently used energy-loss straggling models such as the Lindhard [31] and Chu [57,58] formulas. These models also rely on the FEG approximation but assume a linear interaction between the incoming proton and the medium as well as a simplified description of the target electrons. In addition, the shell-wise local plasma approximation (SLPA) [59], which is also linear and based on FEG, gives results that are close to the Chu formula (not shown here). For all these models the straggling grows as Z_1^2 for increasing projectile charge Z_1. In contrast, the present calculation (TCS-Penn) is nonlinear and provides a better description of the target electrons through the ELF of the material relative to the FEG-based Chu and Lindhard models. The nonlinear effects are indeed small as can be seen from the comparison between TCS-Penn calculations for $Z_1 = 1$ and $Z_1 = 0.1$ shown in Fig. 5. Therefore, nonlinear effects cannot explain the present measured values of energy-loss straggling.

It should be noted that the Yang-O'Connor empirical straggling formula [58] gives much larger straggling results for H^+ on Pt, which agrees with our experimental data for energies below 150 keV but overestimates for larger energies. This formula also provides straggling values much larger than the Chu formula for H^+ projectiles on many different elemental targets [58].

The TCS-Penn approach still underestimates the experimental straggling data. We expect the validity of TCS-Penn calculations for straggling to be somewhat better than for stopping since straggling is dominated by larger momentum transfers, where the dielectric function merges with the Bethe ridge for all models. In addition, possible inaccuracies of the loss function impacted on stopping predictions by around 10% only. Therefore, we believe that any uncertainty of the loss function as far as sum rules are satisfied (as in the present case), will not be able to explain the large underestimation by TCS-Penn calculations of the observed straggling. Moreover, the remaining differences are well reproduced by the bunching effect as calculated from Eq. (8). In this way, the bunching effect is identified to be mainly responsible for the observed augmented straggling values in Pt. This should hold true for other heavy target elements, where the electrons are bunched over many different shells.

V. CONCLUSION

In this work we measured the stopping power and energy-loss straggling for backscattered H^+ on Pt films as a function of the projectile energy by using the MEIS technique. Two sets of samples with different thicknesses were used and the experiments were performed at two different MEIS facilities. In addition, two models were applied to simulate the MEIS spectra. The first one assumes only a single large-angle elastic deflection (v-shape) and the second one is based on full Monte Carlo simulations (full MC). The stopping power and energy-straggling values were extracted from the full MC simulations, because only the MC simulation could reproduce the low-energy measurement accurately. Moreover, we have proposed a model for the energy-loss straggling based on TCS calculations for an inhomogeneous electron system by using the Penn scheme and added the corresponding bunching effect.

Our measurements of the stopping power of protons on Pt agree with recent Moro, Bauer, and Primetzhofer [60] measurements, which were at variance by about 20% with previous measurements and SRIM calculations. The theoretical model TCS-Penn agrees with our stopping measurements for energies lower than 80 keV (in agreement with Refs. [50,60]).

The measured energy-loss straggling values are much larger than the results from the Chu [57,58] and Lindhard [31] models. In contrast, the TCS-Penn calculations for straggling plus an additional term describing bunching effects agree with the present energy-loss straggling measurements and, in particular, shows the importance of bunching effects in the description of the energy-loss straggling at low and medium projectile energies. This is crucial to characterize with ion scattering the shape and elemental depth profile in nanostructures and thin films with Pt, both of which are employed in the catalysis field.

ACKNOWLEDGMENTS

This study was financed in part by: Coordenação de Aperfeiçoamento de Pessoal de Nível Superior - Brazil (CAPES) - Finance Code 001; Conselho Nacional de Desenvolvimento Cientfico e Tecnológico - Brazil (CNPq) Projects No. 141833/2017-3, No. 160018/2019-6, No. 406750/2016-5 and No. 404301/2016-9; and PRONEX-FAPERGS. J.M., P.L.G., and F.F.S. acknowledge support by RADIATE project under the Grant Agreement 824096 from the EU Research and Innovation program HORIZON 2020. M.V. acknowledges the Australian Research Council - Australia (ARC) funding program for financial support. P.L.G. and F.F.S. acknowledge D. Primetzhofer for the enlightening discussions.

[1] J. R. Tesmer and M. A. Nastasi, *Handbook of Modern Ion Beam Materials Analysis*, 1st ed. (Materials Research Society, Pittsburgh, 1995).

[2] W. D. Newhauser and R. Zhang, The physics of proton therapy, Phys. Med. Biol. **60**, R155 (2015).

[3] D. P. Woodruff, D. Brown, P. D. Quinn, T. C. Q. Noakes, and P. Bailey, Structure determination of surface adsorption and surface alloy phases using medium energy ion scattering, Nucl. Instrum. Methods Phys. Res., Sect. B **183**, 128 (2001).

[4] A. A. Demkov and A. Navrotsky, *Materials Fundamentals of Gate Dielectrics* (Springer, Dordrecht, 2005), Vol. 256.

[5] D. F. Sanchez, R. Moiraghi, F. P. Cometto, M. A. Pérez, P. F. Fichtner, and P. L. Grande, Morphological and compositional characteristics of bimetallic core@shell nanoparticles revealed by MEIS, Appl. Surf. Sci. **330**, 164 (2015).

[6] V. Z. C. Paes, M. V. Castegnaro, D. L. Baptista, P. L. Grande, and J. Morais, Unveiling the inner structure of PtPd nanoparticles, J. Phys. Chem. C **121**, 19461 (2017).

[7] International atomic energy agency, electronic stopping power of matter ions, https://www-nds.iaea.org/stopping/.

[8] N. Imanaka and T. Masui, Advances in direct NO_x decomposition catalysts, Appl. Catal., A **431**, 1 (2012).

[9] S. Roy, M. S. Hegde, and G. Madras, Catalysis for NO_x abatement, Appl. Energy **86**, 2283 (2009).

[10] S. M. Shubeita, R. C. Fadanelli, J. F. Dias, and P. L. Grande, Determination of film thicknesses through the breakup of H_2^+ ions, Surf. Sci. **608**, 292 (2013).

[11] H. Trombini, I. Alencar, G. G. Marmitt, R. C. Fadanelli, P. L. Grande, M. Vos, and J. G. England, Profiling As plasma doped Si/SiO_2 with molecular ions, Thin Solid Films **692**, 137536 (2019).

[12] L. F. d. S. Rosa, P. L. Grande, J. F. Dias, R. C. Fadanelli, and M. Vos, Neutralization and wake effects on the Coulomb explosion of swift H_2^+ ions traversing thin films, Phys. Rev. A **91**, 042704 (2015).

[13] E. P. Kanter, P. J. Cooney, D. S. Gemmell, K. O. Groeneveld, W. J. Pietsch, A. J. Ratkowski, Z. Vager, and B. J. Zabransky, Role of excited electronic states in the interactions of fast (MeV) molecular ions with solids and gases, Phys. Rev. A **20**, 834 (1979).

[14] M. Vos and P. L. Grande, Extension schemes of the dielectric function, and their implications for ion stopping calculations, J. Phys. Chem. Solids **133**, 187 (2019).

[15] P. Sigmund, *Particle Penetration and Radiation Effects* (Springer, Berlin, 2014), Vol. 2.

[16] See supplemental material at http://link.aps.org/supplemental/10.1103/PhysRevA.102.032812 for sample characterization and all analyzed MEIS spectra.

[17] M. Mayer, SIMNRA, a simulation program for the analysis of NRA, RBS and ERDA, in *The fifteenth international conference on the application of accelerators in research and industry*, edited by J. L. Duggan, B. Stippec, and I. Lon Morgan, AIP Conf. Porc. No. 475 (AIP, New York, 1999), p. 541.

[18] C. Wang, P. Brault, and T. Sauvage, Density measurement of W thin films coating by combination of ion beam analysis and scanning electron microscopy, Eur. Phys. J.: Appl. Phys. **31**, 17 (2005).

[19] M. Samuelsson, D. Lundin, J. Jensen, M. A. Raadu, J. T. Gudmundsson, and U. Helmersson, On the film density using high power impulse magnetron sputtering, Surf. Coat. Technol. **205**, 591 (2010).

[20] R. G. Smeenk, R. M. Tromp, H. H. Kersten, A. J. H. Boerboom, and F. W. Saris, Angle resolved detection of charged particles with a novel type toroidal electrostatic analyser, Nucl. Instrum. Methods Phys. Res. **195**, 581 (1982).

[21] R. M. Tromp, H. H. Kersten, E. Granneman, F. W. Saris, R. Koudijs, and W. J. Kilsdonk, A new UHV system for channeling/blocking analysis of solid surfaces and interfaces, Nucl. Instrum. Methods Phys. Res., Sect. B **4**, 155 (1984).

[22] M. A. Sortica, P. L. Grande, G. Machado, and L. Miotti, Characterization of nanoparticles through medium-energy ion scattering, J. Appl. Phys. **106**, 114320 (2009).

[23] G. G. Marmitt, PowerMEIS-3 simulation code; http://tars.if.ufrgs.br/.

[24] G. G. Marmitt, Ph.D. thesis, Universidade Federal do Rio Grande do Sul, Porto Alegre, 2017 (unpublished); https://lume.ufrgs.br/handle/10183/170451.

[25] J. B. Marion and F. C. Young, *Nuclear Reaction Analysis, Graphs and Tables* (North-Holland Publishing Company, Amsterdam, 1968).

[26] P. Sigmund, *Particle Penetration and Radiation Effects* (Springer-Verlag, Berlin, Heidelberg, Heidelberg, 2006), Vol. 1.

[27] P. L. Grande, Alternative treatment for the energy-transfer and transport cross section in dressed electron-ion binary collisions, Phys. Rev. A **94**, 042704 (2016).

[28] M. A. Sortica, V. Paneta, B. Bruckner, S. Lohmann, T. Nyberg, P. Bauer, and D. Primetzhofer, On the Z_1-dependence of electronic stopping in TiN, Sci. Rep. **9**, 176 (2019).

[29] F. Matias, P. L. Grande, M. Vos, P. Koval, N. E. Koval, and N. R. Arista, Nonlinear stopping effects of slow ions in a no-free-electron system: Titanium nitride, Phys. Rev. A **100**, 030701(R) (2019).

[30] E. Bonderup and P. Hvelplund, Stopping power and energy straggling for swift protons, Phys. Rev. A **4**, 562 (1971).

[31] J. Lindhard and M. Scharff, *Energy Loss in Matter by Fast Particles of Low Charge*, Mathematical-Physical Announcements The Royal Danish Society of Sciences (Copenhagen: The Royal Danish Academy of Sciences and Letters, 1953), Vol. 15, p. 27.

[32] D. R. Penn, Electron mean-free-path calculations using a model dielectric function, Phys. Rev. B **35**, 482 (1987).

[33] F. Matias, R. C. Fadanelli, P. L. Grande, N. E. Koval, R. Díez Muiño, A. G. Borisov, N. R. Arista, and G. Schiwietz, Ground- and excited-state scattering potentials for the stopping of protons in an electron gas, J. Phys. B: At., Mol. Opt. Phys. **50**, 185201 (2017).

[34] A. F. Lifschitz and N. R. Arista, Velocity-dependent screening in metals, Phys. Rev. A **57**, 200 (1998).

[35] J. Lindhard and A. H. Sørensen, Relativistic theory of stopping for heavy ions, Phys. Rev. A **53**, 2443 (1996).

[36] P. Sigmund, Kinetic theory of particle stopping in a medium with internal motion, Phys. Rev. A **26**, 2497 (1982).

[37] W. Werner, K. Glantschnig, and C. Ambrosch-Draxl, Optical constants and inelastic electron-scattering data for 17 elemental metals, J. Phys. Chem. Ref. Data **38**, 1013 (2009).

[38] Y. Sun, H. Xu, B. Da, S. feng Mao, and Z. jun Ding, Calculations of energy-loss function for 26 materials, Chin. J. Chem. Phys. **29**, 663 (2016).

[39] J. H. Weaver, Optical properties of Rh, Pd, Ir, and Pt, Phys. Rev. B **11**, 1416 (1975).

[40] W. R. Hunter, D. W. Angel, and G. Hass, Optical properties of evaporated platinum films in the vacuum ultraviolet from 220 Å to 150 Å, J. Opt. Soc. Am. **69**, 1695 (1979).

[41] B. Henke, E. Gullikson, and J. Davis, X-ray interactions: Photoabsorption, scattering, transmission, and reflection at $E =$ 50–30, 000 eV, $Z =$ 1–92, At. Data Nucl. Data Tables **54**, 181 (1993).

[42] F. Besenbacher, J. Andersen, and E. Bonderup, Straggling in energy loss of energetic hydrogen and helium ions, Nucl. Instrum. Methods **168**, 1 (1980).

[43] P. L. Grande and G. Schiwietz, Impact-parameter dependence of electronic energy loss and straggling of incident bare ions on H and He atoms by using the coupled-channel method, Phys. Rev. A **44**, 2984 (1991).

[44] J. H. R. dos Santos, P. L. Grande, M. Behar, J. F. Dias, N. R. Arista, J. C. Eckardt, and G. H. Lantschner, Experimental energy straggling of protons in SiO_2, Phys. Rev. A **68**, 042903 (2003)..

[45] P. Sigmund and A. Schinner, Impact-parameter-dependent stopping of swift ions - iii. bunching and packing in energy-loss straggling, Eur. Phys. J. D **58**, 105 (2010).

[46] P. L. Grande and G. Schiwietz, Convolution approximation for swift particles, CasP program, free download from http://www.casp-program.org/ (2006).

[47] T. Krist and P. Mertens, Proton energies at the maximum of the electronic stopping cross section in materials with $57 \leqslant Z_2 \leqslant 83$, Nucl. Instrum. Methods Phys. Res. **218**, 790 (1983).

[48] T. Krist and P. Mertens, Stopping ratios for 30-330 keV light ions in materials with $57 \leqslant Z_2 \leqslant 83$, Nucl. Instrum. Methods Phys. Res. **218**, 821 (1983).

[49] E. Sirotinin, A. Tulinov, V. Khodyrev, and V. Mizgulin, Proton energy loss in solids, Nucl. Instrum. Methods Phys. Res., Sect. B **4**, 337 (1984).

[50] D. Primetzhofer, Inelastic energy loss of medium energy H and He ions in Au and Pt: Deviations from velocity proportionality, Phys. Rev. B **86**, 094102 (2012).

[51] D. Goebl, D. Roth, and P. Bauer, Role of *d* electrons in electronic stopping of slow light ions, Phys. Rev. A **87**, 062903 (2013).

[52] C. E. Celedón, E. A. Sánchez, L. Salazar Alarcón, J. Guimpel, A. Cortés, P. Vargas, and N. R. Arista, Band structure effects in the energy loss of low-energy protons and deuterons in thin films of Pt, Nucl. Instrum. Methods Phys. Res., Sect. B **360**, 103 (2015).

[53] M. J. Berger, M. Inokuti, H. H. Andersen, H. Bichsel, D. Powers, S. M. Seltzer, D. Thwaites, and D. E. Watt, Jour-

nal of the International Commission on Radiation Units and Measurements, ICRU Report 49, Vol. os25, p. NP, doi: 10.1093/jicru/os25.2.Report49.

[54] J. F. Ziegler, M. Ziegler, and J. Biersack, SRIM - The stopping and range of ions in matter (2010), Nucl. Instrum. Methods Phys. Res., Sect. B **268**, 1818 (2010).

[55] J. F. Ziegler, SRIM-2013 software package, http://www.srim.org (2013).

[56] Y. Kido and T. Koshikawa, Energy straggling for medium-energy H^+ beams penetrating Cu, Ag, and Pt, Phys. Rev. A **44**, 1759 (1991).

[57] W. Chu, Calculation of energy straggling for protons and helium ions, Phys. Rev. A **13**, 2057 (1976).

[58] Q. Yang, D. O'Connor, and Z. Wang, Empirical formulas for energy loss straggling of ions in matter, Nucl. Instrum. Methods Phys. Res., Sect. B **61**, 149 (1991).

[59] C. C. Montanari and J. E. Miraglia, The energy loss straggling of low Z ions in solids and gases, in *Application of Accelerations in Research and Industry : Twenty-Second International Conference*, edited by J. Xiao, J. Ke, and Z. You, AIP Conf. Proc. No. 1525 (AIP, New York, 2013), p. 259.

[60] M. V. Moro, P. Bauer, and D. Primetzhofer, Experimental electronic stopping cross section of transition metals for light ions: Systematics around the stopping maximum, Phys. Rev. A **102**, 022808 (2020).